On the Spiral Structure of NGC 2915 and Dark Matter

M. Bureau[1] and F. S. Masset[2]

[1]Hubble Fellow, Columbia Astrophysics Lab., New York, NY; [2]Service d'Astrophysique, CE-Saclay, France

Abstract

NGC 2915 is a blue compact dwarf (BCD) galaxy embedded in an extended, low surface brightness H I disk with a short bar and extended spiral structure. Bureau et al. (1999) showed that conventional mechanisms are unable to drive this pattern. Using hydrodynamical simulations, we explore here whether a rotating triaxial dark halo (or bar) or disk dark matter offer alternative solutions. The spiral structure can be reproduced by an unseen triaxial halo or bar, but the large halo pattern frequency and bar mass required make this unlikely. In particular, the spin parameter λ is much higher than predicted by current cold dark matter (CDM) structure formation scenarios. The massive disk models develop the proper spiral structure when the surface density is scaled up by a factor of 10, suggesting that the disk contains much more mass than is visible, tightly linked to the hydrogen. A classic halo is nevertheless still required to fit the circular velocity curve without making the disk violently unstable. Scaling the surface density profile by ≈ 10 brings the disk and halo masses to comparable values within the disk radius. The surface density remains just under Kennicutt's (1989) star formation threshold for a gas-only disk, as required.

Introduction

NGC 2915 is a nearby BCD galaxy with a high surface brightness star-forming core and a red diffuse population. The H I disk extends to 22 radial scalelengths and displays a short central bar with an extended two-arm spiral (see Fig.1; Meurer et al. 1994, 1996). It is completely dark matter dominated, with $M_T/L_B \gtrsim 65$ and $M_{\rm dark}/M_{\rm luminous} \approx 19$ at the last measured point. Bureau et al. (1999) argued for a slow pattern speed, $\Omega_p = 8.0 \pm 2.4$ km s^{-1} kpc^{-1}, yielding a corotation radius to bar semi-length ratio $r_{\rm cr}/r_b \gtrsim 1.7$, consistent with the idea that bars in dense halos should be slow (e.g. Debattista & Sellwood 1998). Furthermore, NGC 2915's isolation, low surface density, and pseudo-rings locations argue against interactions, swing amplification, or bar-driving generating the observed pattern.

Models

Here, we use hydrodynamical simulations to test two alternative mechanisms: i) the H I disk is embedded in an extended triaxial dark halo (or bar) with a rotating figure, forcing the pattern at a certain frequency, or ii) (some) dark matter is in a disk following closely the H I, rendering the disk gravitationally unstable. The code is a simple 2D Eulerian finite difference program on a polar mesh, with self-gravity. We assume that the disk dynamics can be modeled with an isothermal gas disk in which the sound speed c_s is everywhere equal to the velocity dispersion, $c_s \equiv \sigma_v$, but we also did runs with $c_s \equiv 8$ km s^{-1}.

The dark halo and bar are imposed by rotating triaxial potentials, the exact profiles of which are unimportant as their torques are mostly received at the resonances. We use for the bar an exponentially declining density profile stratified on generalized ellipsoids, and for the halo a pure $m = 2$ potential with a flat tangential to radial accelation ratio. The massive disk models are obtained by simply scaling up the (axisymmetrized) gaseous surface density of the disk and adding a small $m = 2$ seed. To prevent fragmentation for large scalings (low Q), we filter out all modes except the $m = 0$, 2, 4, and 6. In all cases, another axisymmetric potential is added to match the circular velocity curve.

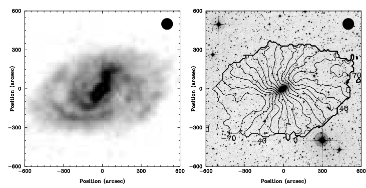

Figure 1: Left: Greyscale rendering of the naturally-weighted total H I map of NGC 2915. **Right:** H I velocity field overlaid on a DSS optical image. The 45″ round beam is shown in the top-right corner of both maps (Meurer et al. 1996).

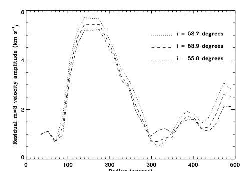

Figure 2: Amplitude of the $m = 3$ component of the deprojected velocity field of NGC 2915 as a function of radius, for three different values of the assumed inclination. $i = 53^\circ\!.9$ (*dashed line*) is adopted.

Constraints

Linear Regime: The basic constraints are provided by the density and velocity fields, but we refine these. The dispersion relation for an m-folded density wave in an isothermal disk is, in the WKB limit:

$$m^2(\Omega - \Omega_p)^2 = \kappa^2 - 2\pi G\Sigma_g|k| + k^2c_s^2\,, \tag{1}$$

where $k^2 = m^2/r^2 + k_r^2$, k_r is the radial wave vector, Σ_g the surface density, Ω_p the pattern frequency, Ω the orbital frequency (v_c/r), and κ the epicyclic frequency. Once Ω_p is fixed, k (and thus k_r) follows, and k_r is related to the pitch-angle β of the spiral by $\tan\beta = m/k_r r$. In the linear regime, one thus only needs to adjust the imposed frequency to match the observed pitch angle; the perturber's strength can be adjusted independently to match the arm-interarm contrast. In NGC 2915, where the disk response is non-linear and full simulations are required, these values act as a guide.

Simulations: For a thin disk, the observed velocity field is:

$$v = [-u\cos(\theta - \varphi) + v\sin(\theta - \varphi)]\sin i\,, \tag{2}$$

where u and v are the radial and azimuthal velocities in the galaxy rest frame, i the inclination, and θ and φ the azimuth of the fluid element considered and of the observer. As the velocity field associated with an m-folded density wave has an $e^{im\theta}$ dependence, it leads to $m - 1$ and $m + 1$ folded signatures in the deprojected perturbed field.

It is impossible to disentangle which fraction of the $m = 1$ deprojected velocity comes from an $m = 2$ wave or from a warp, so we discard the $m = 1$ information for NGC 2915. The $m = 3$ signature is reliable, however, and is only affected by an error in the inclination, which we can minimize. We thus adopt it as our main constraint for the models (see Fig. 2) and implement it by maximizing a properly defined correlation coefficient χ (between $V_3^{\rm obs}(r)$ and $V_3^{\rm sim}(r)$) in both time t and observer azimuth φ.

Triaxial Halo Models

Results and Discussion

Figures 3–4 show the best bar forcing runs, with pattern frequencies $5.0 - 7.5$ km s^{-1} kpc^{-1}. A tentative bar mass was first adopted for each run and the best match in both time t and observer's azimuth φ identified. A second simulation was then run scaled by the inverse of the ratio

$$\mathcal{S} = \frac{\int_0^{r_{\rm ext}} r V_3^{\rm sim}\, dr}{\int_0^{r_{\rm ext}} r V_3^{\rm obs}\, dr}\,, \tag{3}$$

resulting in bar masses $M_b = 4.7 - 6.8 \times 10^9\ M_\odot$.

The pattern speeds fitting well $V_3^{\rm obs}(r)$ and the total H I map are very well constrained, $\Omega_p \approx 5.5 - 6.5$ km s^{-1} kpc^{-1}, but the isovelocities north of the center exhibit an unobserved twist and the main spiral in the outer disk is not reproduced at all. As the maximal mass one can assign to the visible component of NGC 2915 is about $8.0 \times 10^8\ M_\odot$, the imposed bars must be dark. The triaxial halo runs give similar results, with $\Omega_p \approx 6.5 - 8.0$ km s^{-1} kpc^{-1} and axis ratios $a/b \approx 0.83 - 0.88$.

The inferred range of pattern frequencies is roughly consistent with the direct measurement by Bureau et al. (1999) and implies a slow bar, with corotation near the edge of the H I disk ($r_{\rm cr}/r_b \approx 2.8$). Together with NGC 2915's unusually dense and compact halo (Meurer et al. 1996), this is consistent with models of dark matter dominated (i.e. sub-maximal) barred galaxies, where bars transfer most of their angular momenta to the halos (e.g. Debattista & Sellwood 1998).

The same dark potentials can simultaneously account for the arm-interarm contrast and the amplitude of the $V_3^{\rm obs}(r)$ profile. However, COBE-normalized ΛCDM simulations only yield mildly flattened and triaxial halos, with highly concentrated halos (and the halos' outer regions) being more spherical (e.g. Jing & Suto 2002). This argues against strong triaxiality in NGC 2915, although the probability distribution is maximum for axis ratios of $0.83 - 0.88$, as measured.

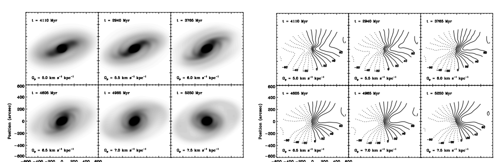

Figure 3: Left: Synthetic column density maps for the best bar forcing runs. **Right:** Synthetic velocity fields. The timestep and pattern frequency are indicated in each panel.

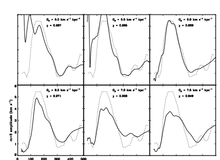

Figure 4: Amplitude of the $m = 3$ component of the deprojected velocity field as a function of radius, for the best bar forcing runs. *Solid lines:* models. *Dotted lines:* observations. The pattern frequency and correlation coefficient χ are indicated in each panel.

Figure Rotation

The figure rotation of triaxial halos in CDM simulations has not been studied, but the pattern frequency inferred here is probably too high. The modified halo spin parameter $\lambda' \equiv J/\sqrt{2}MVR$, where J is the angular momentum inside a sphere of radius R, containing mass M, and $V = \sqrt{GM/R}$ (Bullock et al. 2001). Assuming spherical symmetry and neglecting the dark particles' motion in the rotating frame,

$$\lambda' = \frac{\sqrt{2}\,\Omega_p \int_0^R \frac{dM}{dr} r^2 dr}{3MVR}\,. \tag{4}$$

As the statistics of λ' is robust to the choice of R, we choose the outer disk radius, where corotation occurs ($\Omega_p R/V \approx 1$). This leads to $\lambda' > \lambda'_{\rm min} = \sqrt{2}/9 \approx 0.157$.

For λ''s log-normal distribution with $\lambda'_0 = 0.035 \pm 0.005$ and $\sigma = 0.5 \pm 0.03$ (Bullock et al. 2001), the probability that a halo has a spin parameter as large as $\lambda'_{\rm min}$ is at best 5×10^{-3}, and more realistic estimates yield 1.6×10^{-4}. So unless there are sizable net internal streaming motions which cancel almost perfectly our estimate of J, it is unlikely that the perturbing potential can be a rotating halo. A considerable fraction of the halo total energy would otherwise be in rotational kinetic energy ($\frac{1}{2}J\Omega_p$).

In fact, we can make an order of magnitude estimate of the maximum pattern frequency for any halo with extended triaxiality: $\Omega_{\rm vir} \sim V_{\rm vir}/R_{\rm vir}$, corresponding to a bar with half-length equal to the halo virial radius $R_{\rm vir}$ and $r_{\rm cr}/r_{\rm b} = 1$. Given that $M_{\rm vir} \approx 200 \times \frac{4}{3}\pi R_{\rm vir}^3\,\rho_{\rm crit}$ and $H^2 = \frac{8\pi G}{3}\rho_{\rm crit}$ (where H is Hubble's constant and $\rho_{\rm crit}$ the critical density),

$$\Omega_{\rm vir} \sim 10\,H\,. \tag{5}$$

Triaxial figure pattern frequencies should thus be largely independent of the halo virial mass. For $H = 70$ km s^{-1} Mpc^{-1}, $\Omega_{\rm vir} \sim 0.7$ km s^{-1} kpc^{-1} and $T_{\rm fig} = 2\pi/\Omega_{\rm vir} \sim 9$ Gyr, in good agreement with the preliminary work of Bureau et al. (1999) but an order of magnitude lower than required for NGC 2915.

Heavy Disk Models

Results and Discussion

As Toomre's parameters $X(r) = r\kappa^2/2\pi m G\Sigma$ and $Q(r) = c_s\kappa/\pi G\Sigma$ are everywhere well above their critical values, a global disk instability requires more disk mass than is observationally inferred. Like many objects, the gaseous surface density of NGC 2915 closely follows the total mass distribution (mostly dark), and we simply scale it up by a uniform factor $\lambda_\Sigma \geq 1$.

We use a three-step procedure to find the range where a grand-design spiral similar to that of NGC 2915 develops: i) for a given scaling factor λ_Σ, we evaluate at each instant t the observer's azimuth φ that maximizes the correlation coefficient χ; ii) given $\varphi(t)$, we calculate the relative perturbation amplitude $\mathcal{S}(t)$ (eq. 3) and its time average $\overline{\mathcal{S}}(\lambda_\Sigma)$; iii) we vary λ_Σ until $\overline{\mathcal{S}}(\lambda_\Sigma) \approx 1$, a perfect match (see Fig. 5).

The time average $\overline{\mathcal{S}}(\lambda_\Sigma)$ depends dramatically on the scaling, so λ_Σ is tightly constrained. The best match occurs for $\lambda_\Sigma = 4.93$ and Figure 6 shows the corresponding density and velocity fields, as well as the $m = 3$ component of the deprojected velocity field ($V_3^{\rm sim}(r)$). Although the model is not strongly bar-like in the center, it reproduces the tightly wrapped spiral arms in the outer parts, where triaxial models fail. We can thus account for most of the large-scale structure of NGC 2915 by simply scaling up its gas content. The agreement is superb considering the dimensionality (1) of the parameter space!

To account for finite thickness, the disk surface densities must be corrected by a factor

$$q \approx (1 + kH) \approx \left(1 + \frac{2\sigma_v}{v_c\tan\beta}\right) \approx 2.0\,, \tag{6}$$

where H is the characteristic disk thickness. A vertically resolved disk will thus have a surface density an order of magnitude higher than observed ($\Sigma'_g(r) = q\lambda_\Sigma\,\Sigma_g(r) \approx 10\,\Sigma_g(r)$), such that the integrated masses of the halo and disk are roughly equal over most of the disk and the halo dominates further out (see Fig. 7). This agrees with recent ΛCDM structure formation simulations with gas cooling and the values derived for a number of spiral galaxies (e.g. Hoekstra et al. 2001; Teyssier 2002).

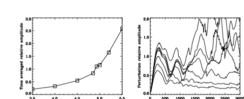

Figure 5: Left: Time-averaged relative amplitude $\overline{\mathcal{S}}(\lambda_\Sigma)$ as a function of the scaling factor λ_Σ for the heavy disk models. **Right:** Time dependence of $\mathcal{S}(t)$ for various values of λ_Σ (identified in the left panel). The thick line represents the best match model, with $\lambda_\Sigma = 4.93$.

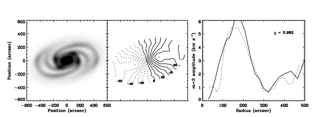

Figure 6: Left: Synthetic column density map for the best heavy disk model. **Center:** Velocity field. **Right:** $m = 3$ component of the deprojected velocity field. *Solid line:* model. *Dotted line:* observations.

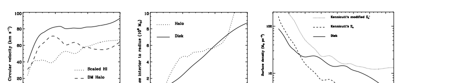

Figure 7: Left: Circular velocity curve decomposition for the best heavy disk model. *Dotted line:* heavy disk. *Dashed line:* dark halo. *Solid line:* total. **Center:** Cumulative mass profiles of the heavy disk (*solid line*) and halo (*dotted line*). **Right:** Surface densities of the heavy disk (*solid line*), Kennicutt's critical star formation threshold (*dashed line*), and our modified threshold (*dotted line*).

Disk Properties:

Fitting NGC 2915's circular velocity curve with a heavy disk only would require a scaling factor $\lambda_\Sigma \approx 25$, but it would yield a poor fit (see Fig. 7) and the resulting disk would be violently unstable ($Q \ll 1$). This strongly argues for the presence of a classical dark matter halo in addition to any realistic massive disk. A similar argument could be made based on the number of spiral arms (Athanassoula et al. 1987).

It is also informative to compare the heavy disk surface density with Kennicutt's (1989) threshold for star formation. For a purely gaseous disk, the equivalent condition reads

$$\Sigma'_{\rm crit}(r) = \frac{2\kappa\sigma_v}{\pi G}\,, \tag{7}$$

about 3.2 times higher than Kennicutt's standard (two-component, gas and stars) criterion. According to this modified criterion, the scaled up disk is not expected to form stars at all, as required by observations, but it would at almost all radii according to the standard one (see Fig. 7). The heavy disk surface density profile is thus everywhere close to but smaller than $\Sigma'_c(r)$, and NGC 2915 appears as an aborted optical grand-design spiral. The non-prediction of star formation in the center is caused by our neglect of the stellar component, extending to about 3 kpc.

Q and thus λ_Σ also directly depend on the assumed velocity dispersion of the dark disk material. The ratio c_s/Σ_g (or σ_v/Σ_g) is degenerate in the expression of Q, and less additional material would be needed for a lower assumed dispersion.

If, in any isolated object, the increased surface density required to explain a spiral pattern were to over-predict the circular velocity curve, disk dark matter (exclusively) could be ruled out. Undisturbed low surface brightness galaxies that are not dark matter dominated but show a clear spiral structure would be ideal candidates, but it is not clear if they exist.

Acknowledgements: Support for this work was provided by NASA through Hubble Fellowship grant HST-HF-01136.01 awarded by STScI, which is operated by AURA, Inc., for NASA, under contract NAS 5-26555.